

# Desynchronization Index: A New Connectivity Approach for Exploring Epileptogenic Networks

FEDERICO MASON\*, Department of Information Engineering, University of Padova, Italy

LORENZO FERRI\*, IRCCS Institute of Neurological Sciences of Bologna, Full Member of European Reference Network EpiCare, Italy

LIDIA DI VITO, IRCCS Institute of Neurological Sciences of Bologna, Full Member of European Reference Network EpiCare, Italy

LARA ALVISI, Department of Neuromotor and Biomedical Sciences, University of Bologna, Italy

LUCA ZANUTTINI, Department of Neuromotor and Biomedical Sciences, University of Bologna, Italy

MATTEO MARTINONI, IRCCS Institute of Neurological Sciences of Bologna, Full Member of European Reference Network EpiCare, Italy

ROBERTO MAI, Centro Munari Chirurgia dell'Epilessia e del Parkinson, Niguarda Hospital, Italy

FRANCESCO CARDINALE, Centro Munari Chirurgia dell'Epilessia e del Parkinson, Niguarda Hospital, Italy and Department of Medicine and Surgery, Unit of Neuroscience, University of Parma, Italy

PAOLO TINUPER, Department of Neuromotor and Biomedical Sciences, University of Bologna, Italy

ROBERTO MICHELUCCI, IRCCS Institute of Neurological Sciences of Bologna, Full Member of European Reference Network EpiCare, Italy

ELENA PASINI<sup>†</sup>, IRCCS Institute of Neurological Sciences of Bologna, Full Member of European Reference Network EpiCare, Italy

FRANCESCA BISULLI<sup>†</sup>, IRCCS Institute of Neurological Sciences of Bologna, Full Member of European Reference Network EpiCare, Italy and Department of Neuromotor and Biomedical Sciences, University of Bologna, Italy

---

\*These authors are both corresponding.

<sup>†</sup>These authors equally contributed.

---

Authors' Contact Information: Federico Mason, federico.mason@unipd.it, Department of Information Engineering, University of Padova, Padova, Italy; Lorenzo Ferri, lorenzo.ferri@ausl.bologna.it, IRCCS Institute of Neurological Sciences of Bologna, Full Member of European Reference Network EpiCare, Bologna, Italy; Lidia Di Vito, lidia.divito@ausl.bologna.it, IRCCS Institute of Neurological Sciences of Bologna, Full Member of European Reference Network EpiCare, Bologna, Italy; Lara Alvisi, lara.alvisi@unibo.it, Department of Neuromotor and Biomedical Sciences, University of Bologna, Bologna, Italy; Luca Zanuttini, luca.zanuttini@studio.unibo.it, Department of Neuromotor and Biomedical Sciences, University of Bologna, Bologna, Italy; Matteo Martinoni, m.martinoni@isnb.it, IRCCS Institute of Neurological Sciences of Bologna, Full Member of European Reference Network EpiCare, Bologna, Italy; Roberto Mai, roberto.mai@ospedaleniguarda.it, Centro Munari Chirurgia dell'Epilessia e del Parkinson, Niguarda Hospital, Milan, Italy; Francesco Cardinale, francesco.cardinale@ospedaleniguarda.it, Centro Munari Chirurgia dell'Epilessia e del Parkinson, Niguarda Hospital, Milan, Italy and Department of Medicine and Surgery, Unit of Neuroscience, University of Parma, Parma, Italy; Paolo Tinuper, paolo.tinuper@unibo.it, Department of Neuromotor and Biomedical Sciences, University of Bologna, Bologna, Italy; Roberto Michelucci, roberto.michelucci@isnb.it, IRCCS Institute of Neurological Sciences of Bologna, Full Member of European Reference Network EpiCare, Bologna, Italy; Elena Pasini, elena.pasini@isnb.it, IRCCS Institute of Neurological Sciences of Bologna, Full Member of European Reference Network EpiCare, Bologna, Italy; Francesca Bisulli, francesca.bisulli@unibo.it, IRCCS Institute of Neurological Sciences of Bologna, Full Member of European Reference Network EpiCare, Bologna, Italy and Department of Neuromotor and Biomedical Sciences, University of Bologna, Bologna, Italy.

---

Permission to make digital or hard copies of all or part of this work for personal or classroom use is granted without fee provided that copies are not made or distributed for profit or commercial advantage and that copies bear this notice and the full citation on the first page. Copyrights for components of this work owned by others than the author(s) must be honored. Abstracting with credit is permitted. To copy

In this work, we propose a new computational framework to assist neurophysiologists in Stereoelectroencephalography (SEEG) analysis, with the final aim of improving the definition of the Epileptogenic Zone (EZ) in patients with drug-resistant epilepsy. We design a new algorithm, named Desynchronization Index (DI), that classifies as most epileptogenic those SEEG channels that show independent behavior during the seconds preceding the seizure propagation. We test the proposed DI algorithm against the Epileptogenic Index (EI) algorithm on a clinical dataset of 11 patients, considering the neurophysiological evaluation of the EZ as the clinical ground truth. Our results denote that DI overcomes EI in terms of area under the ROC curve (AUC=0.81 vs AUC=0.74) while combining the two algorithms as a unique tool leads to the best performance (AUC=0.87). The DI algorithm underscores connectivity dynamics that can hardly be identified with a pure visual analysis, increasing the accuracy of the EZ definition compared to traditional methods. This technique can lead to the definition of a new effective biomarker of the EZ, reducing the burden required by the SEEG review in the case of extensive implants and improving our understanding of the dynamics leading to the generation of seizures.

CCS Concepts: • **Applied computing** → **Health informatics**; • **Theory of computation** → *Dynamic graph algorithms*.

Additional Key Words and Phrases: Stereoelectroencephalography, drug-resistant epilepsy, cortical connectivity, time-varying networks, phase transfer entropy.

#### ACM Reference Format:

Federico Mason, Lorenzo Ferri, Lidia Di Vito, Lara Alvisi, Luca Zanuttini, Matteo Martinoni, Roberto Mai, Francesco Cardinale, Paolo Tinuper, Roberto Michelucci, Elena Pasini, and Francesca Bisulli. 2025. Desynchronization Index: A New Connectivity Approach for Exploring Epileptogenic Networks. *ACM Trans. Comput. Healthcare* 1, 1, Article 1 (January 2025), 21 pages. <https://doi.org/XXXXXXXX.XXXXXXX>

## 1 Introduction

The localization of the Epileptogenic Zone (EZ) is the fundamental prerequisite for performing epilepsy surgery in people with drug-resistant epilepsy [34]. Ensuring a higher accuracy in the definition of the EZ makes it possible to reduce the extent of the surgery, mitigating the risk of complications or chronic deficits. In the most complex scenario, the EZ can be identified only through invasive procedures, among which Stereoelectroencephalography (SEEG) represents the most accurate methodology [27]. An SEEG recording involves the surgical implantation of electrodes into the patient's brain, enabling the monitoring of electrical activity from deep cortical regions, which is essential for the identification of the EZ. As a result, SEEG-guided surgical resections lead more than 60% of patients to be seizure-free after the intervention [14]. However, SEEG has the drawback of providing very focused information: if none of the intracranial electrodes intersects the EZ, the procedure may result in an unclear EZ definition and an unsuccessful epilepsy surgery [12].

Nowadays, SEEG interpretation is mainly based on visual analysis, focusing on the early phase of the seizure discharge. The final goal is to define an EZ that can be focal or distributed among multiple cortical structures, a scenario falling under the concept of epileptogenic networks [4]. The above process is particularly complex since SEEG signals include hundreds of components, whose analysis requires the involvement of highly specialized neurophysiologists. For this reason, in the last years, SEEG interpretation has started being supported by computational tools that aim at characterizing the EZ and, more in general, the dynamics leading to seizure generation [18]. The most common methods analyze the SEEG power spectrum, searching for the cortical sites generating *fast oscillations* [41], i.e., electrical activities with frequencies in the gamma range ([30, 100] Hz), as done in the cases of Epileptogenic Index (EI) [5] and Epileptogenic Maps (EMs) [16].

---

otherwise, or republish, to post on servers or to redistribute to lists, requires prior specific permission and/or a fee. Request permissions from [permissions@acm.org](mailto:permissions@acm.org).

© 2025 Copyright held by the owner/author(s). Publication rights licensed to ACM.

ACM 2637-8051/2025/1-ART1

<https://doi.org/XXXXXXXX.XXXXXXX>

Another approach is to model cortical connectivity with the aim of identifying which brain structures show abnormal connectivity behavior during seizure onset. In this context, the first studies analyzed the responses generated through intracranial stimulations, known as Cortico-Cortical Evoked Potentials (CCEPs) [10], which, however, do not have a physiological origin and may not correctly represent cortical connectivity patterns. Other solutions estimate the exchange of information by analyzing the phase distribution of the signals associated with each cortical site, as performed by the Phase Locking Value (PLV) and the Phase Lag Index (PLI). These methods avoid biases associated with amplitude differences within the signal recordings but only allow us to estimate the synchrony between different signals, which results in a functional connectivity model. To estimate the direction of neural connections, it is necessary to use more advanced methodologies such as the Phase Transfer Entropy (PTE) which, however, was applied to SEEG data only in a limited number of cases.

Although multiple quantitative approaches have been developed for the study of epileptogenic networks, the literature often presents discordant findings. Most works agree that the *ictal phase* (i.e., the period that involves the epileptic discharge) is preceded by a reduction in cortical connectivity, followed by the opposite phenomenon during the seizure propagation [40]. Recently, it has been hypothesized that the EZ presents an abnormal inward information flow during the inter-ictal phase [20], and the epileptogenic level of each cortical site can be assessed by the connection exerted during seizures [37].

In this work, we present a new framework for supporting neurophysiologists in SEEG interpretation. Specifically, we design a connectivity-based algorithm, named Desynchronization Index (DI), that exploits the PTE to estimate the relations between brain structures and detect connectivity anomalies in the resulting time-varying network. According to our approach, the EZ is identified by the cortical sites that present an independent behavior during the ictal phase. Overall, the main contributions of this manuscript consist of the following points:

- we design a new connectivity-based metric, named *desynchronization level*, describing the tendency for a cortical site to be disconnected from the rest of the brain;
- we design a new algorithm, named DI, which estimates the epileptogenic degree of cortical sites according to their connectivity dynamics, quantified in terms of desynchronization level;
- we implement the DI algorithm to analyze seizure data in 11 consecutive patients with drug-resistant epilepsy who underwent SEEG monitoring;
- we analyze the clinical utility of our method and its main disadvantages and drawbacks in comparison to the EI algorithm and clinical ground truth.

Our results indicate that the combined use of the DI and EI algorithms can offer important support to neurophysiologists for the identification of the EZ. In particular, the DI algorithm underscores anomalous connectivity dynamics which can hardly be detected by adopting a pure visual analysis or by using EI as a standalone tool. Thus, the proposed technique may be used to identify cortical regions that, despite not presenting fast oscillations, surround the EZ and play an active role in the generation and propagation of seizures.

## 2 Related Work

In clinical practice, the interpretation of SEEG recordings is mainly based on visual analysis and constitutes a highly time-consuming process because of the huge number of data that must be reviewed [6]. The most common marker of the seizure onset is given by low-voltage fast oscillations, which are electrical discharges spanning beta frequencies ([13, 30] Hz), usually observed in mesial temporal seizures, and gamma frequencies ([30, 100] Hz), observed in neocortical seizures. To quantify the magnitude of fast oscillations and the network dynamics leading to seizures, it is possible to analyze the spectrum of SEEG signals. This approach is followed by the EI algorithm [5], which is the most routinely used method to assist clinicians in SEEG interpretation [35].

The EI algorithm, occasionally combined with other biomarkers [3], has been recognized to provide the best accuracy in terms of EZ localization and surgical prediction. An extension of such an approach is the

*epileptogenicity rank*, a technique that, before computing the EI values, assigns weights to SEEG sites depending on to their distance from the hypothesized center of the EZ [38]. This solution has the obvious limitation of biasing the epileptogenic levels assigned to each channel by a prior assumption. In particular, the epileptogenicity rank framework reduces the number of false positives when the clinical hypothesis is correct, but it dramatically decreases sensitivity in the other case.

While EI focus on the energy distribution in the frequency domain, other approaches analyze the variation in neuronal connectivity during the ictal phase. Several tools have been proposed to this goal, including the PLV [30] and the PLI [44], with different trade-offs in terms of sensitivity and precision [22]. In particular, the PLI was proposed as an alternative to the PLV in order to mitigate the noisy information associated with the *volume conduction* [39], reducing the number of false positives. A more advanced method is the PTE [33], which exploits the Granger Casuality (GC) [42] to estimate both the delay and the direction of neuronal connections, and constitutes a very promising technique for SEEG analysis [46].

In addition to designing EI, Bartolomei et al. analyze the SEEG data using the nonlinear regression coefficient ( $h_2$ ) [47], and show that the epileptogenic network is associated with reduced connectivity in the period that anticipates the ictal phase [7]. In particular, the  $h_2$  coefficient is agnostic to the signal frequencies, while most connectivity models discern cortical relationships depending on the frequency bands. Following this principle, the authors of [15] estimate connectivity by the cross-correlation between SEEG signals, showing that seizure frequency is proportional to the outward connectivity of epileptogenic channels. Similar methodologies are given in [9], where pairwise correlation is combined with Euclidean distance to estimate the EZ extension, and in [31], where graph theory is exploited to identify the network hubs that contribute the most to seizure propagation.

Recently, the use of Spearman rank correlation [49] to assess the coupling between SEEG signals has shown good results for both the detection of the EZ and the prediction of surgical outcomes [25]. Other connectivity-based approaches associate the phase of slow oscillations ( $< 30$  Hz) with the amplitude of fast oscillations ( $> 30$  Hz), as occurred for the Phase Slope Index (PSI) and the Phase Amplitude Coupling (PAC) [8]. In a recent work [28], the use of PSI allows the authors to show that the EZ presents higher outward connectivity during seizures than in the resting state. Similar results are observed in [32], where SEEG connectivity is estimated via the PAC between the high (gamma) and low (delta and theta) frequency bands. The authors of [1] seem to contradict these findings and, using the Partial Direct Coherence (PDC) [2] as the connectivity model, assess that the EZ presents higher inward connectivity during seizure generation.

In recent years, the popularity of Machine Learning (ML) has encouraged many researchers to apply data-driven techniques to epileptogenic networks [26]. For example, the authors of [21] exploit hypergraph learning to automatically detect SEEG fast oscillations, while [24] investigates different patient-specific ML models for analyzing scalp electroencephalography signals. In addition, [19] exploit a Support Vector Machine (SVM) model to integrate multiple electrophysiological characteristics, including both fast oscillations and low-frequency suppression, to improve accuracy in EZ detection. This supports the hypothesis that ictal channels are not identified by specific frequency components, and more comprehensive methodologies are required to describe the generation of seizures. On the other hand, [19] and similar works consider as ground truth the area resected by epilepsy surgery, which is usually much larger than the EZ to maximize the probability of seizure reduction. In general, the high complexity behind SEEG analysis makes it extremely difficult to build supervised datasets, which prevents ML solutions from obtaining reliable performance in this field [48].

Although the large variety of works implementing connectivity-based metrics for the interpretation of SEEG, the results of the literature do not lead to an agreement on which biomarkers characterize EZ. Initial studies show that the ictal transition is characterized by a reduction in connectivity, but the EZ is often identified by cortical sites with a greater coupling during seizure propagation. In this work, we try to answer these questions by quantifying the level of epileptogenicity of SEEG sites in terms of *desynchronization*. With the latter, we denote

the tendency of a cortical site to show independent electrical behavior that cannot be inhibited by neighboring brain structures.

### 3 Analytical Model

In this section, we first describe how SEEG signals are modeled within our framework and introduce the EI algorithm, which represents the state-of-the-art for detecting the EZ. Then, we present the connectivity model used to infer the relation between SEEG sites starting from their phase distribution. Finally, we introduce the DI algorithm, which evaluates the epileptogenicity level of each site according to its tendency to isolate itself from the network.

#### 3.1 Epileptogenic Index

We model a single SEEG recording as a multidimensional signal with  $N$  different components, named *channels*, one for each cortical site analyzed. In the following, we denote by  $\mathcal{N}$  the set of channels and by  $|\cdot|$  the cardinality operator, so that the number of cortical sites is equal to  $N = |\mathcal{N}|$ . According to our approach, each channel  $x \in \mathcal{N}$  is segmented in multiple overlapping windows  $x(t)$ , with  $t = 0, \Delta t, 2\Delta t, \dots$ , where  $\Delta t$  represents the time-shift between consecutive windows. Given the window duration  $T_{\text{window}}$  and the sampling frequency  $f_s$ , the sample number per window is  $n = T_{\text{window}}/f_s$ .

The EI algorithm requires to evaluate the signal energy in the frequency domain [5]. Given a specific window  $x(t)$ , the algorithm first computes the Fourier Transform (FT) of  $x(t)$ , obtaining a complex value  $X(t, f)$  for each frequency in  $[0, f_s/2]$ . Hence, the *energy ratio* between the high- and low-frequency bands of the target signal  $x$  is computed as

$$E_x(t) = \frac{\int_{B_h} \|X(t, f)\|^2 df}{\int_{B_\ell} \|X(t, f)\|^2 df}, \quad (1)$$

where  $B_h$  and  $B_\ell$  are the high- and low-frequency ranges, while  $\|\cdot\|$  is the norm function. The straightforward idea behind this technique is that epileptic discharge is characterized by the increase of fast oscillations, which are assessed in terms of energy ratio. Normalizing the high-frequency by the low-frequency energy, it is possible to compare signals recorded in different cortical sites, which may be characterized by different amplitude and, thus, energy distribution. At the same time, computing the energy ratio is not sufficient to determine the EZ: there may be channels that are associated with high energy ratio values even in the absence of epileptic discharges.

To avoid the underlined issue, the EI algorithm considers a CUMulative SUM (CUSUM) control chart to discern the channels with abrupt increases in the energy ratio. Given a sequence of observations  $\omega(t)$ , interspersed by a period  $\Delta t$ , the CUSUM control chart is defined by the function

$$\Gamma(\omega, t) = \begin{cases} \max \left\{ 0, \Gamma(\omega, t - \Delta t) + \frac{\omega(t) - \mu_\omega}{\sigma_\omega} - \gamma \right\}, & t > 0; \\ \omega(t), & t = 0; \end{cases} \quad (2)$$

where  $\gamma$  is a tuning parameter that makes the statistic less or more sensitive to the new observations, while  $\mu_\omega$  and  $\sigma_\omega$  are the estimates of the mean and standard deviation of  $\omega$ . In the case of the EI algorithm, the observations  $\omega(t)$  are given by the energy ratio  $E_x$  associated with each channel  $x \in \mathcal{N}$ .

The original version of the EI algorithm does not consider the standard deviation  $\sigma_{E_x}$  in the normalization and dynamically re-estimates the mean  $\mu_{E_x}$  every time the energy ratio varies significantly. Instead, in this work, we propose to estimate both the  $\mu_{E_x}$  and  $\sigma_{E_x}$  statistic by looking at the period immediately preceding the ictal discharge. Practically, for each channel  $x \in \mathcal{N}$ , we compute  $\mu_{E_x}$  and  $\sigma_{E_x}$  over the time interval  $[t_{\text{base}}, t_{\text{start}}]$ , where  $t_{\text{start}}$  is the instant at which the epileptic discharge starts to form. Then, we compute the cumulative sum  $\Gamma(E_x, t)$

of the energy ratio  $E_x$  for each time  $t \in [t_{\text{start}}, t_{\text{end}}]$ , where  $t_{\text{end}}$  is the instant at which the epileptic discharge propagates within the overall network.

Given a channel  $x \in \mathcal{N}$  and  $\Gamma(E_x, t), \forall t \in [t_{\text{start}}, t_{\text{end}}]$ , we define the *activation time*  $t_{E_x}$  of the channel as the time instant at which  $\Gamma(E_x, t)$  reaches the highest value:

$$t_{E_x} = \arg \max_{t \in [t_{\text{start}}, t_{\text{end}}]} \Gamma(E_x, t) \quad (3)$$

Besides, we define the *tonicity*  $c_{E_x}$  of the channel as the sum of the energy ratio  $E_x$  computed over the interval following the channel's activation time:

$$c_{E_x} = \int_{t_{E_x}}^{t_{E_x} + \delta} E_x(t) dt, \quad (4)$$

where  $\delta$  is a tuning parameter determining the interval over which  $c_{E_x}$  is computed.

Hence, we can select the  $M$  channels with strongest energy ratio changes by defining the set  $\mathcal{N}_E \subset \mathcal{N}$ , of cardinality  $|\mathcal{N}_E| = M$ , whose elements  $y$  comply with the conditions

$$\Gamma(E_y, t_{E_y}) > \Gamma(E_x, t_{E_x}), \forall x \in \mathcal{N} \setminus \mathcal{N}_E. \quad (5)$$

Under this perspective,  $M$  denotes the maximum number of epileptogenic channels that are detected by the algorithm. The EI value of each channel  $x \in \mathcal{N}_E$  is then given by

$$EI_x = \frac{c_{E_x}}{t_{E_x} - t_{\text{start}}}, \quad (6)$$

while the EI value of each channel  $x \in \mathcal{N} \setminus \mathcal{N}_E$  is set to 0. We observe that  $EI_x$  is proportional to  $c_{E_x}$  and decreases as a function of the time difference between the channel activation time  $t_{E_x}$  and the beginning of the ictal phase  $t_{\text{start}}$ .

The above formulation stands out from the original EI algorithm by reducing the number of parameters to be manually set. In particular,  $t_{\text{start}}$  and  $t_{\text{end}}$  denote the period during which the epileptic discharge takes shapes. Instead,  $t_{\text{base}}$  should be defined in such a way to ensure that the statistics  $\mu_{E_x}$  and  $\sigma_{E_x}$  are as accurate as possible. Hence, the only parameters to be tuned are the maximum number  $M$  of epileptogenic channels, the interval  $\delta$  over which the tonicity is computed, and the weight  $\gamma$  of the CUSUM control chart, which trades off between the false alarm and miss-detection probabilities.

### 3.2 Effective Connectivity Model

To estimate the information flows within the SEEG network, we consider the PTE algorithm, which, given a couple of channels  $x, y \in \mathcal{N}$  at time  $t$ , models their coupling according to their phase distributions. Given a specific window  $x(t)$ , we first compute its *analytic representation*  $X(t) = x(t) + HT(x(t))$ , where  $HT(\cdot)$  is the Hilbert transform. We observe that  $X(t)$  is associated with  $n = T_{\text{window}}/f_s$  phase values, representing the evolution of the *instantaneous phase*  $\theta_x(t)$  of  $x(t)$  in time.

As next step, we need to model the phase distribution: in this work, we follow the Sturges rule [17] and compute the bin width of  $\theta_x(t)$  as  $\vartheta = 2\pi/(\log_2(n) + 1)$ . This quantization process allows us to reduce the influence of volume conduction on the connectivity model. A similar principle is adopted by the PLI, which, however, does not consider the direction of the information flows between neural signals [44]. In addition, PLI underestimates the neural connections associated with small propagation delays or whose phase difference distribution fluctuates around zero. The opposite approach is taken by the PLV, which model the phase in a continuous domain and, consequently, suffers more the problems associated with volume conduction. By varying the number of phase bins in our model, we can trade off between specificity and sensitivity, similar to what occurs when using the PLI instead of the PLV.

Let us denote by  $\theta_x(t)$  and  $\theta_y(t)$  the phase distribution of  $x(t)$  and  $y(t)$ , respectively. According to the PTE algorithm, the connectivity that the channel  $x$  exerts on the channel  $y$  at time  $t$ , considering a lag  $\tau$ , is given by

$$T_{x \rightarrow y}(t, \tau) = H(\theta_y(t), \theta_y(t + \tau)) + H(\theta_x(t), \theta_y(t)) - H(\theta_x(t), \theta_y(t), \theta_y(t + \tau)) - H(\theta_y(t)), \quad (7)$$

where  $H(\cdot)$  denotes the entropy function. We observe that the PTE, as reported in (7), is a directed connectivity measure, which means that, in general,  $T_{x \rightarrow y}(t, \tau) \neq T_{y \rightarrow x}(t, \tau)$ . In order to remove the dependency from  $\tau$ , with a slight abuse of notation, we redefine the phase transfer entropy between  $x(t)$  and  $y(t)$  as the maximum value of  $T_{x \rightarrow y}(t, \tau)$  among multiple lags in the set  $[0, \tau_{max}]$ :

$$T_{x \rightarrow y}(t) = \max_{\tau \in [0, \tau_{max}]} T_{x \rightarrow y}(t, \tau). \quad (8)$$

By doing so, we obtain that the magnitude of the effective connection exerted on the channel  $y$  by the channel  $x$  at time  $t$  is given by  $T_{x \rightarrow y}(t)$ , while the propagation delay associated with such a connection is:

$$\tau_{x \rightarrow y}(t) = \arg \max_{\tau \in [0, \tau_{max}]} T_{x \rightarrow y}(t, \tau). \quad (9)$$

Hence, if  $\tau_{x \rightarrow y}(t) = 0$ , there is a zero propagation delay for the information flow going from  $x(t)$  to  $y(t)$ .

### 3.3 Desynchronization Index

To identify ictal channels from the connectivity analysis, we follow a similar approach to that presented in [43], where Sparks and colleagues extended the Exponentially Weighted Moving Average (EWMA) statistic to detect anomalous behaviors in time-varying networks. In particular, we assume that the generation of epileptic discharges is associated with an abrupt reduction in the communication between the EZ and the rest of the cortical structures.

Given a sequence of observations  $\omega(t)$ , interspersed by a period  $\Delta t$ , the EWMA control chart is defined by the function:

$$\mathcal{E}(\omega, t) = \begin{cases} \alpha \omega(t) + (1 - \alpha) \mathcal{E}(\omega, t - \Delta t) & t > 0; \\ \omega(t) & t = 0; \end{cases} \quad (10)$$

where  $\alpha \in [0, 1]$  is a tuning parameter that determines the rate at which older information influences the EWMA statistic. In particular, as  $\alpha \rightarrow 1$ , the function gives more importance to the most recent observations, better capturing rapid changes in the process at the cost of an increased false alarm probability.

In the following, we write  $\mathcal{T}(t)$  to indicate the distribution of the inter-channel connections  $T_{x \rightarrow y}(t), \forall x, y \in \mathcal{N}$ , at time  $t$ . Hence, we denote by  $M[\mathcal{T}(t)]$ ,  $P_{75}[\mathcal{T}(t)]$ , and  $P_{25}[\mathcal{T}(t)]$  the median, the 75th percentile, and the 25th percentile of  $\mathcal{T}(t)$ . We use the EWMA algorithm, as defined in Eq.(10), to compute a smoothed version of the above statistics as well as of each connection  $T_{x \rightarrow y}(t), \forall x, y \in \mathcal{N}$ . Hence, we define  $\mathcal{N}_x^{\text{in}}(t)$  and  $\mathcal{N}_x^{\text{out}}(t)$  as the sets of channels presenting abnormal connectivity toward and from channel  $x$  at time  $t$ :

$$\begin{aligned} \mathcal{N}_x^{\text{in}}(t) &= \{y \in \mathcal{N} : \mathcal{E}(T_{y \rightarrow x}, t) \leq \mathcal{E}(P_{25}[\mathcal{T}], t)\}, \\ \mathcal{N}_x^{\text{out}}(t) &= \{y \in \mathcal{N} : \mathcal{E}(T_{x \rightarrow y}, t) \geq \mathcal{E}(P_{75}[\mathcal{T}], t)\}. \end{aligned} \quad (11)$$

In other words, we consider abnormal those connections that go outside the inter-quartile range of the time-varying network distribution. This, on the one hand, allows us to implicitly customize the framework to each patient without the need to define additional parameters as in [43]. On the other hand, choosing other percentile ranges for discerning abnormal connections could lead to different trade-offs in terms of accuracy, and, in the future, further investigation of how to tune such a parameter is required.

Table 1. Demographic and clinical data.

Patient index	Sex	Age (SEEG)	Age (onset)	Seizure frequency	Epileptogenic zone localization	Propagation zone localization	Surgery	Outcome (1 year)	Histology
1	Male	39	33	Weekly	Right temporal	Temporal	Lobectomy	Seizure free	HS 1
2	Male	24	1	Daily	Left orbito-frontal	Fronto-insular	RF-TC	Seizure reduction	Not available
3	Male	36	16	Monthly	Left temporal	Temporal	Lobectomy	Seizure free	FCD 1b
4	Female	52	3	Weekly	Right temporal	Temporal and FOI	Lobectomy	Seizure free	HS 1
5	Female	25	2	Weekly	Right temporo-basal	Parietal and insular	Lobectomy	Seizure free	Aspecific
6	Male	48	22	Weekly	Right temporal	Fronto-orbito-insular	Lobectomy	Seizure free	HS 1
7	Male	36	9	Weekly	Right temporo-occipital	Temporal	RF-TC	Seizure reduction	Not available
8	Female	49	12	Monthly	Left temporal	Temporo-lateral	Lobectomy	Seizure free	HS 1
9	Male	24	18	Weekly	Right temporal	Temporal	RF-TC	Seizure free	Tumor
10	Female	38	13	Monthly	Right temporo-occipital	Temporo-mesial	RF-TC	Not available	Not available
11	Male	32	1	Monthly	Left temporo-occipital	Insulo-opercular	RF-TC	Not available	Not available

We define the actual  $\psi_x^{\text{in}}(t)$  and expected  $\hat{\psi}_x^{\text{in}}(t)$  inward connection density of channel  $x$  at time  $t$  as

$$\psi_x^{\text{in}}(t) = \sum_{y \in \mathcal{N}_x^{\text{in}}(t)} \mathcal{E}(T_{y \rightarrow x}, t), \quad (12)$$

$$\hat{\psi}_x^{\text{in}}(t) = |\mathcal{N}_x^{\text{in}}(t)| \cdot \mathcal{E}(M[\mathcal{T}], t). \quad (13)$$

In a similar way, we define  $\psi_x^{\text{out}}(t)$  and  $\hat{\psi}_x^{\text{out}}(t)$  as

$$\psi_x^{\text{out}}(t) = \sum_{y \in \mathcal{N}_x^{\text{out}}(t)} \mathcal{E}(T_{x \rightarrow y}, t), \quad (14)$$

$$\hat{\psi}_x^{\text{out}}(t) = |\mathcal{N}_x^{\text{out}}(t)| \cdot \mathcal{E}(M[\mathcal{T}], t). \quad (15)$$

Finally, we define the desynchronization level of channel  $x \in \mathcal{N}$  at time  $t$  as

$$D_x(t) = \frac{\sqrt{\hat{\psi}_x^{\text{in}}(t)} - \sqrt{\psi_x^{\text{in}}(t)}}{\sqrt{\psi_x^{\text{out}}(t)} - \sqrt{\hat{\psi}_x^{\text{out}}(t)}}, \quad (16)$$

where the square root operator is used to stabilize the variance of the process [43]. The numerator of the above equation depends on the inward connection of  $x$ , while the denominator refers to the influence that  $x$  exerts on other channels. Hence,  $D_x(t)$  represents the tendency of  $x$  to self-isolate from the rest of the network.

We apply the CUSUM chart to the desynchronization level, thus obtaining  $\Gamma(D_x, t)$  for each channel  $x \in \mathcal{N}$  and for each time  $t \in [t_{\text{start}}, t_{\text{end}}]$ . Hence, using equations (3) and (4), we can compute the activation times  $t_{D_x}$  and the tonicities  $c_{D_x}$ ,  $\forall x \in \mathcal{N}$ , considering the desynchronization level instead of the energy ratio. Following the same approach presented in 3.1, we define the set  $\mathcal{N}_D$ , including the  $M$  channels showing the strongest changes in terms of connectivity. Finally, for each channel in  $\mathcal{N}_D$ , we define the DI values as

$$DI_x = \begin{cases} \frac{c_{D_x}}{t_{D_x} - t_{\text{start}}} & x \in \mathcal{N}_D, \\ 0 & x \notin \mathcal{N}_D. \end{cases} \quad (17)$$

The DI algorithm follows the same settings of EI, making it necessary to tune only the maximum number  $M$  of epileptogenic channels, the interval  $\delta$ , and the weight  $\gamma$ .



## 4 Evaluation Methodology

In this section, we present the clinical dataset in which our tool is evaluated, describing the SEEG recording process and the patient characteristics. Then, we showcase how the EI and DI algorithms are implemented and describe how we evaluate their performance in the detection of the EZ.

### 4.1 Clinical Dataset

This study considers a cohort of 12 consecutive patients that were monitored through SEEG at the IRCCS Institute of Neurological Sciences of Bologna from January 2022 to June 2024. The study protocol was approved by the local ethics committee (protocol number 741-2021, committee code 97338), and written informed consent was obtained from each patient. In all cases, the SEEG implant included multiple electrodes, each presenting 5–18 recording sites, named contacts; the number and location of the electrodes were patient-tailored, while each contact was 22 mm in length, and separated by 1.5 m from neighboring contacts.

The SEEG implantation followed the workflow developed at Niguarda Hospital [11], which involves the construction of a multimodal scene of the patient’s brain. The scene allows for a comprehensive evaluation of all the anatomical information regarding the cortical area explored by each contact. The SEEG signals were recorded using the Nihon Kohden 2100 polygraph, considering 192 or 256 channels and a sampling frequency of  $f_s = 1000$  Hz. High-definition synchronized videos were recorded for the whole duration of each SEEG monitoring (up to 20 days per patient), enabling a correlation between electrical and clinical features. Finally, we collected the main demographic and clinical data of each patient, including age at disease onset, seizure semiology, neuropsychological examinations, neuroimaging findings, scalp EEG recordings, surgical outcomes, follow-up information, and histopathological diagnoses.

From the initial dataset, a single patient was excluded as the SEEG record did not allow the localization of the EZ and no epilepsy surgery was performed. The final cohort comprises 7 males and 4 females with an average age of 36.6 years (range 24-49) at the recording time, and 8.8 years (range 1-22) at the disease onset. Clinical data indicated a probable EZ in the temporal lobe in 7 cases (5 right, 2 left), in the left frontal lobe in a single case, and in the temporo-occipital lobe in the remaining cases (2 right, 1 left). Radiofrequency thermocoagulations allowed control of seizures in a single patient, while the remaining patients underwent anterior-temporal lobectomy. Histopathological analysis led to clinical results compatible with hippocampal sclerosis in 4, and cortical dysplasia in 1 cases. Demographic and clinical details of the studied population are reported in Tab. 1<sup>1</sup>.

### 4.2 Performance Evaluation

For each patient, we consider the channels belonging to the EZ as the detection target. The selection of the EZ channels was performed by two board-certified neurophysiologists (L.D-V. and E.P.), who were blinded to the output of our computational framework. We selected a single seizure per patient and analyzed an SEEG epoch of  $T_{\text{epoch}} = 200$  seconds for each seizure, considering the period before the complete diffusion of epileptic discharge. If multiple seizures were available, we discarded the seizures recorded during the first two days of the monitoring period (during which the pharmacological treatment is still active) and those occurring during a cluster of seizures.

Before running the EI and DI algorithms, the SEEG signals were pre-processed through a comb filter centered at  $f_{\text{comb}} = 50$  Hz to remove the powerline frequency and its harmonics. In the analysis, we excluded sites that explore the White Matter (WM) since they are not sources of electric signals. The selection of the WM channels was performed by a board-certified neurophysiologist (L.F.), according to the electrical activity of the cortical

<sup>1</sup>In the table, HS stays for hippocampal sclerosis FCD for focal cortical dysplasia, RF-TC for radio-frequency thermocoagulation, FOI for fronto-orbito-insular.

sites and their location on the multimodal scene. No other cortical sites were excluded, making our framework agnostic to the specific patient and seizure to be analyzed.

The output of the EI and DI algorithms is normalized in the  $[0, 1]$  interval, and a threshold  $\eta$  (in the same range) is set to classify a channel as epileptogenic. Hence, we consider the following performance metrics:

- *sensitivity* (or *true positive rate*), which is the ratio between the number of channels correctly classified as epileptogenic by the algorithm and the total number of epileptogenic channels in the SEEG implant;
- *precision* (or *positive predictive value*), which is the ratio between the number of channels correctly classified as epileptogenic by the algorithm and the total number of channels classified as epileptogenic by the algorithm;
- *accuracy*, which is the ratio between the number of channels correctly classified (as epileptogenic or not epileptogenic) by the algorithm and the total number of channels in the SEEG implant.

In addition, we study the trade-off between sensitivity and precision by computing the Receiver Operating Characteristic (ROC) and the Area Under the ROC Curve (AUC). The AUC is a common performance indicator for diagnostic tools: in clinical settings, a value higher than 0.80 is solely required for obtain a reliable solution [23]. Practically, for each patient, the ROC curve is obtained by varying the number  $M$  of epileptogenic channels up to the size of the SEEG implant.

The EI and DI algorithms are both implemented as standalone tools or combined according to the “and” and “or” Boolean functions. Practically, in the first case (named “EI and DI”), a channel is classified as epileptogenic only if both the algorithms mark it as positive. Instead, in the second case (named “EI or DI”), a channel is classified as epileptogenic if at least one of the algorithms classifies it as positive. Clearly, we expect the first configuration to return less false positives, and the second configuration to provide higher sensitivity.

We observe that other works in this field consider as ground truth the area resected after epilepsy surgery or the target of thermocoagulation treatment. However, using this information does not ensure an accurate EZ definition as, notably, epilepsy surgery is designed to remove a larger area than the sole EZ. In this work, we defined the EZ according to the neurophysiological evaluation of the same SEEG records taken as input by our computational framework. This allows us to evaluate the EI and DI algorithms in fairly context, i.e., during the clinical stage in which it is expected to be used, against a pure human analysis.

## 5 Results

In this section, we present the results obtained by exploiting the EI and DI algorithms for detecting the EZ, considering the performance metrics given in Sec. 4.2. Our computational framework is publicly available at the link: [https://github.com/masonfed/desync\\_index](https://github.com/masonfed/desync_index). At the end of the section, we review in more detail two specific seizures among those analyzed, comparing the algorithm outcomes with clinical observations.

### 5.1 Detection Results

The SEEG signals are segmented in overlapping time windows lasting  $T_{\text{window}} = 1.00$  s each, considering a time shift of  $\Delta t = 0.25$  s between consecutive windows. Given the epoch duration ( $T_{\text{epoch}} = 200$  s) a total of 797 windows is analyzed for each seizure. To estimate the connectivity between different channels according to the PTE algorithm, we consider  $\tau_{\text{max}} = 0.10$  s as the maximum propagation delay. Instead, for computing the energy ratio, the high and low frequency ranges are set to  $B_h = [30.0, 250.0]$  Hz and  $B_\ell = [4.0, 12.0]$  Hz, respectively. This setting extends the portion of the spectrum processed by the EI algorithm, which, in its initial version, considered frequencies lower than 97 Hz [5]. Here, we consider a wider frequency range to capture *ripple* phenomena that are notably characterized by oscillations up to 250 Hz or even more [45].

We set the tonicity interval to  $\delta = 5.00$  s (as done in [5]), the weight of the CUSUM chart to  $\gamma = 0.0$ , and the exponential decay of the EWMA chart to  $\alpha = 1.0$ , following the recommendations provided in [36]. We set

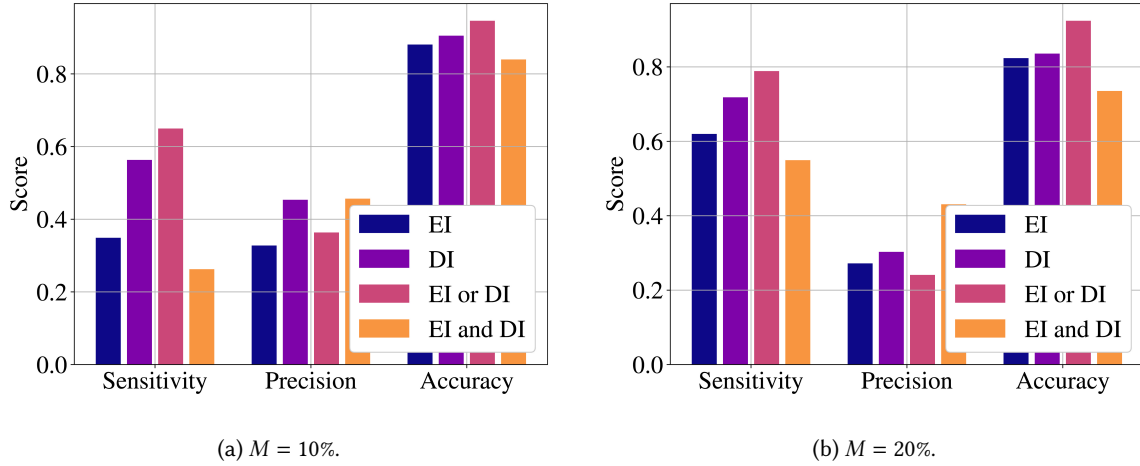


Fig. 1. Performance metrics in the EZ detection.

the detection threshold of the algorithms to  $\eta = 0.0$ , which means that no channels were discarded from the algorithm output and the number of epileptogenic channels is always equal to  $M$ . Finally, we set the baseline period of the CUSUM chart to  $t_{\text{base}} = t_{\text{start}} - 20.0$  s so that the energy and connectivity statistics of each channel are estimating according to the 20.0 s preceding the onset of the seizure. As explained in Sec. 4,  $t_{\text{start}}$  and  $t_{\text{end}}$  depend on the specific seizure analyzed and, therefore, are epoch-tailored.

In Fig. 1a, we report the detection performance of the different algorithms, considering the channels within the EZ as a classification target. In particular, we tune  $M$  is such a way 10% of the channels are considered epileptogenic. We note that DI has higher sensitivity than EI (0.56 and 0.35, respectively), while the "EI or DI" configuration increases the sensitivity more than 50% with respect EI (with a final score of 0.65). This denotes that two algorithms return different results, i.e., the channels associated with a higher EI value are not the same associated with a higher DI value. Focusing on precision, the DI algorithm still overcomes EI (0.45 vs 0.33), while considering the "and" function does not improve the performance than when using DI. The best accuracy is obtained using the "EI or DI" approach, which returns a score of 0.95, followed by the DI algorithm at second place.

To improve sensitivity, we can increase the number  $M$  of channels returned by the algorithms. When we set  $M = 20\%$ , the sensitivity of the "EI or DI" approach reaches a value of 0.79 while the accuracy decreases to 0.92 due to the higher number of false positives (Fig. 1b). On the other hand, we highlight that the main advantage of our technique is to build a first sketch of EZ, allowing neurophysiologists to look at a limited number of channels relative to the original network. This may be strongly beneficial in the case of extensive SEEG implants (with hundreds of channels), where understanding the time-varying dynamics that lead to seizures is extremely difficult with pure visual analysis.

To comprehensively analyze the trade-off between sensitivity and specificity, we vary the value of  $M$  from 1% to 100% and compute the AUC associated with each technique. In particular,  $M = 100\%$  represents the extreme scenario in which all SEEG channels are marked as epileptogenic and neurophysiologists must look at the SEEG records from scratch. In this perspective, we may consider  $M$  as a marker of the effort that neurophysiologists must exert and, therefore, the effectiveness of our framework.

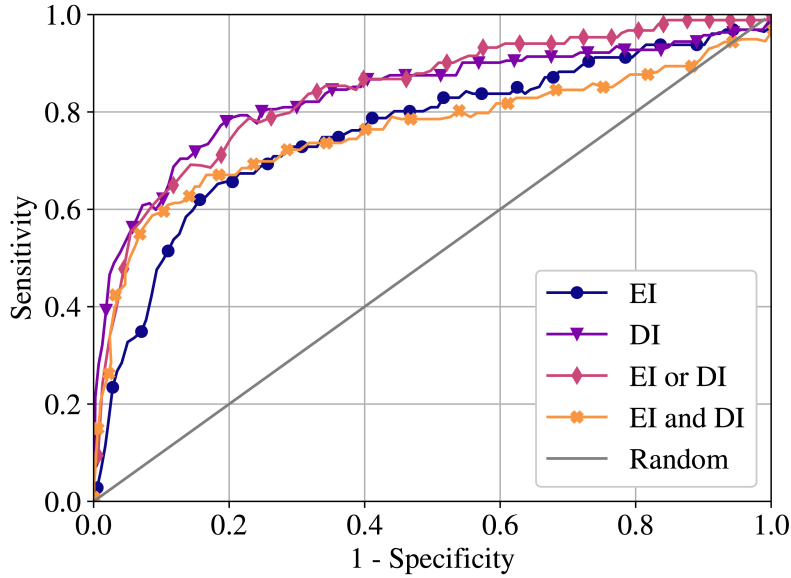
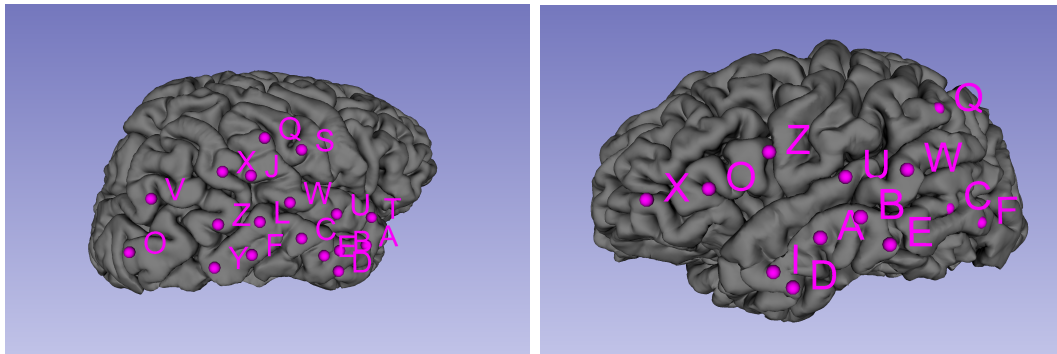


Fig. 2. Area Under the ROC Curve (AUC) in the EZ detection.



(a) Patient 7.

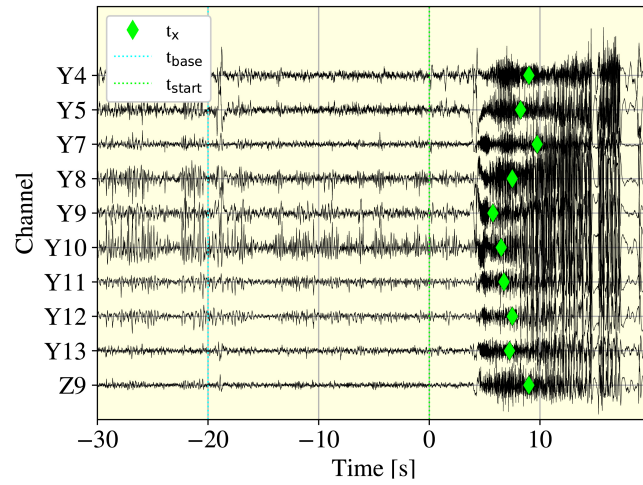
(b) Patient 8.

Fig. 3. SEEG implants.

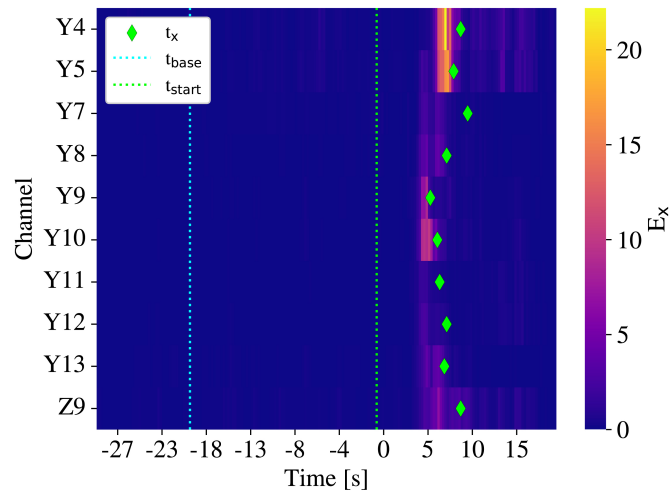
Fig. 2 denotes how the "EI or DI" approach leads to the best detection performance ( $AUC = 0.87$ ), followed by the DI algorithm ( $AUC = 0.81$ ) and the EI algorithm ( $AUC = 0.74$ ) at third place. These results confirm that the combined use of EI and DI enables a more holistic analysis of the overall ictal transition, allowing us to identify most of the channels that are part of the EZ. On the other hand, to ensure a sensitivity close to 0.8, we must still look at more than  $M = 20\%$  of the SEEG channels (as we observed in Fig. 1b). We expect that integration of the proposed tools with other quantitative features, for example, taking into account the space position of recording sites within the implant, can further enhance detection performance. In a clinical setting, this will

make it possible to further reduce the neurophysiologist effort, i.e., the number  $M$  of channels to be individually evaluated.

## 5.2 Concordant Example



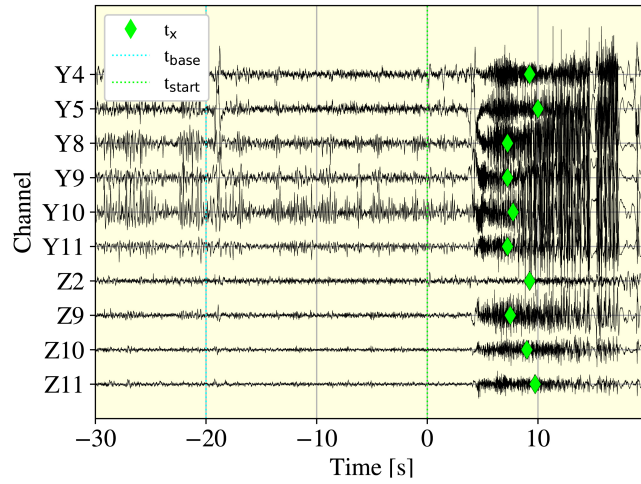
(a) Signal.



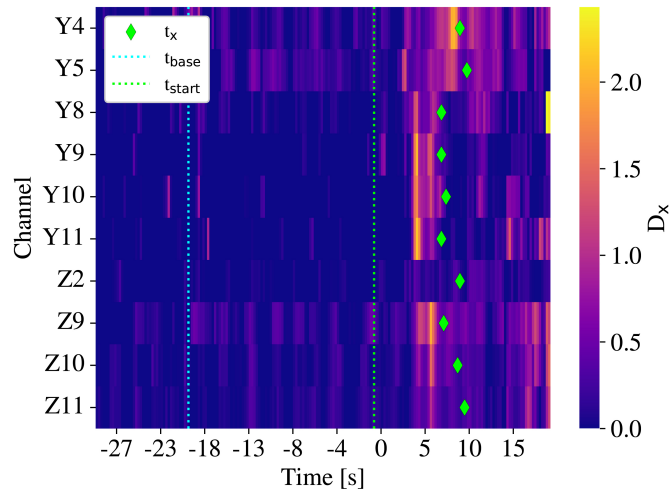
(b) Energy ratio.

Fig. 4. EI operation in a concordant case (patient 7).

In the following, we better evaluate the operations of the two algorithms, analyzing two specific seizure events. In the first case, the two algorithms return concordant outcomes and, thus, identify the same channels as the most



(a) Signal.



(b) Desynchronization level.

Fig. 5. DI operation in a concordant case (patient 7).

epileptogenic. In the second case, the algorithms' results are different, which denotes the importance of integrating different methods for the EZ localization. We first consider patient 7, whose SEEG implant (represented in Fig. 3a) explored the right temporo-parieto-occipital area, and includes 152 different recording sites (18 electrodes). In Fig. 4a, we report the bipolar representation of the  $M = 10$  channels associated with the strongest variation in the energy ratio during the 50 seconds preceding the propagation of epileptic discharges. Instead, in Fig. 4b, we report the energy ratio values associated with each channel.

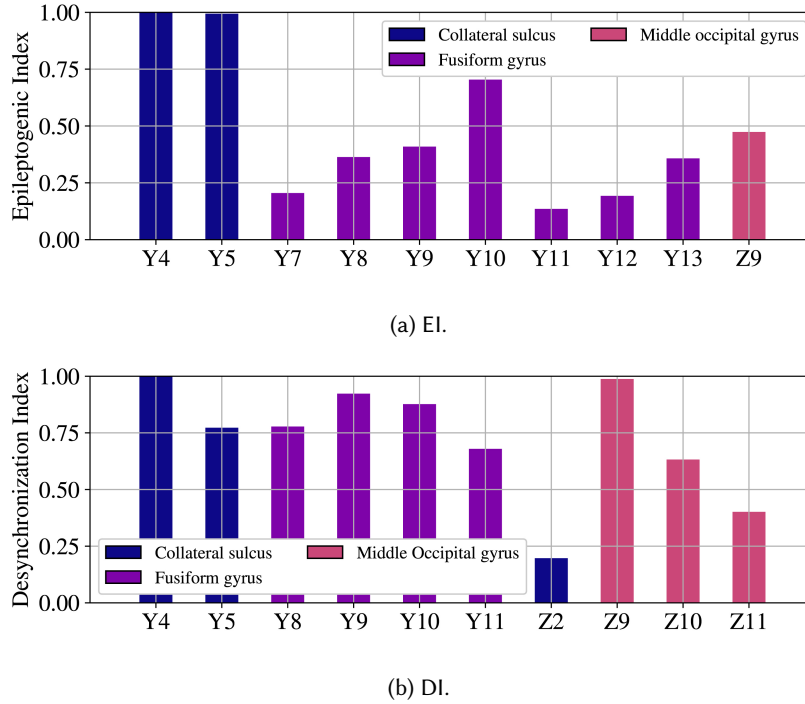


Fig. 6. EI and DI outcomes in a concordant case (patient 7).

In the two figures, the time is shifted according to the start of the ictal phase, so that  $t_{\text{start}} = 0$  s and  $t_{\text{base}} = -20$  s. In particular,  $t_{\text{base}}$  denotes the instant from which the baseline statistics of the energy ratio per channel were calculated,  $t_{\text{base}}$  denotes the instant from which the algorithm starts detecting signal abnormalities, while the markers  $t_x$  denote the activation times, i.e., the times at which the energy ratio  $E_x$  diverges from its baseline.

Looking at Fig. 5, we can analyze the operation of the DI algorithm in the same scenario. Hence, Fig. 5a reports the  $M = 10$  channels showing the most significant connectivity changes, while Fig. 5b) reports the desynchronization level of each channel. Comparing Fig. 5b with Fig. 4b, we can observe that the energy ratio represents a less noisy metric than the desynchronization level. During the baseline, the energy ratio of each channel tends to zero, while, for  $t_{\text{start}} > 0$ , most channels present abrupt energy changes, with a peak  $E_x$  for channels Y4 and Y5. The desynchronization level is characterized by higher variability, and many channels present bursts of reduced connectivity for  $t_{\text{start}} < 0$ . In particular, channels Y4 and Y5 present abnormal connectivity patterns even during the baseline.

Hence, in Fig. 6, we report the epileptogenicity levels assigned to each channel by the two algorithms, as well as the brain structure with which each channel is associated. In both cases, the output of the algorithms is normalized within the  $[0, 1]$  range so that values close to 1 are associated with a greater influence on the diffusion of epileptic discharge. We observe that the outputs are mostly concordant as both techniques identify the most epileptogenic channels within the posterior collateral sulcus and the fusiform gyrus, which were considered triggers of the patient's seizures.

## 5.3 Discordant Example

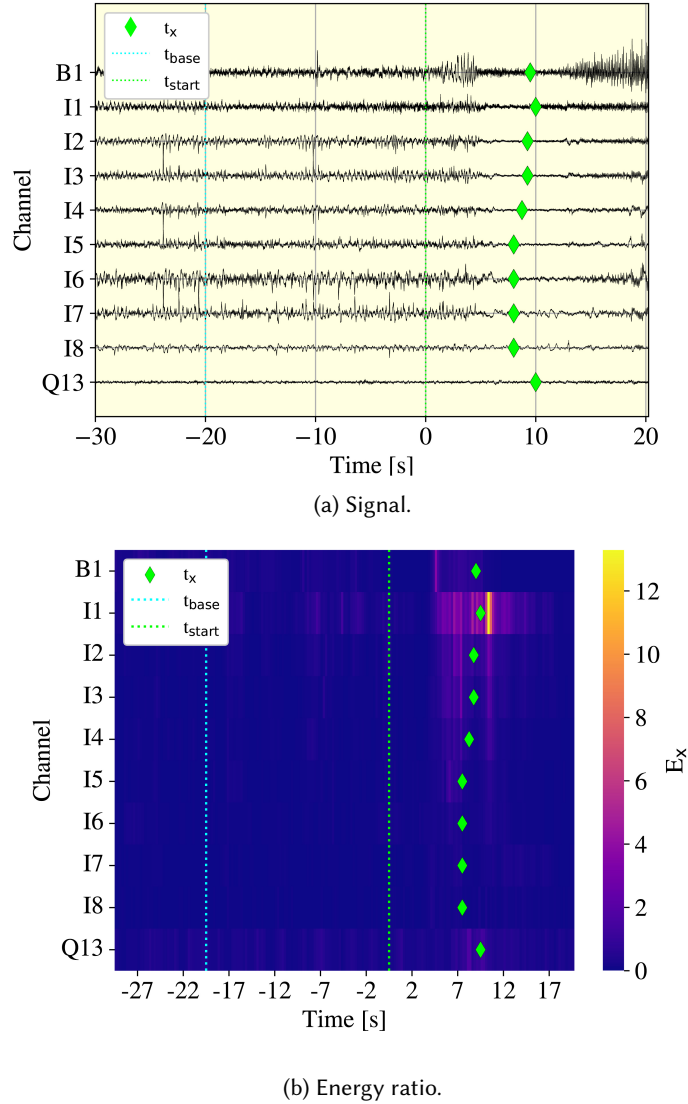
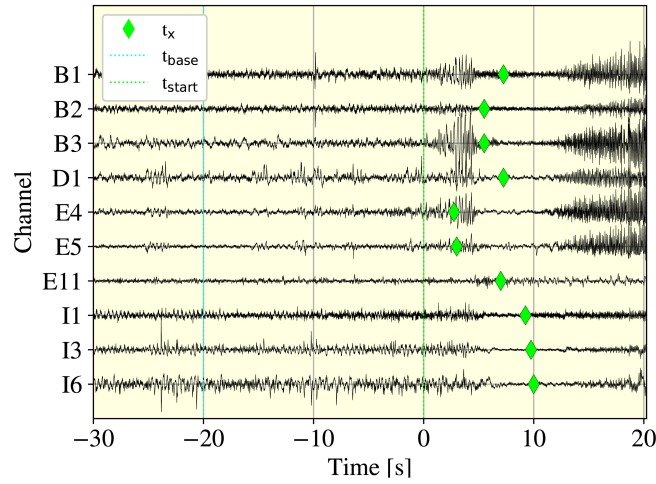


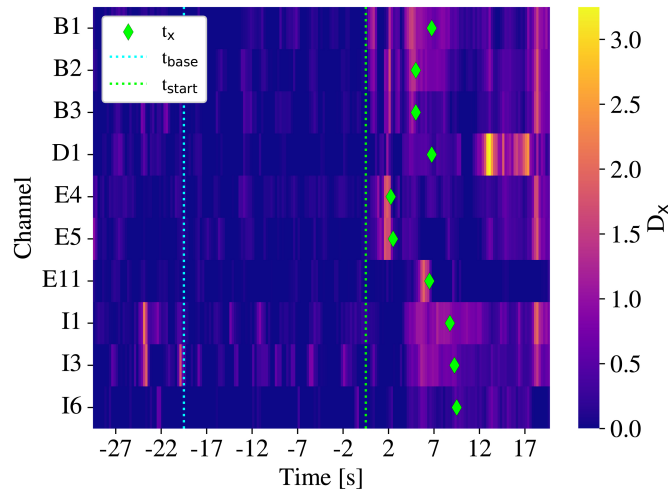
Fig. 7. EI operation in a discordant case (patient 8).

In the following, we consider patient 8, whose SEEG implant (represented in Fig. 3b) explored the left fronto-temporo-parietal, area, and includes 116 recording sites (13 electrodes). We report the  $M = 10$  channels considered the most epileptogenic according to the two approaches, focusing first on the EI algorithm (Fig. 7) and then on the DI algorithm (Fig. 8). As before, the energy ratio associated with each channel presents low values during the





(a) Signal.

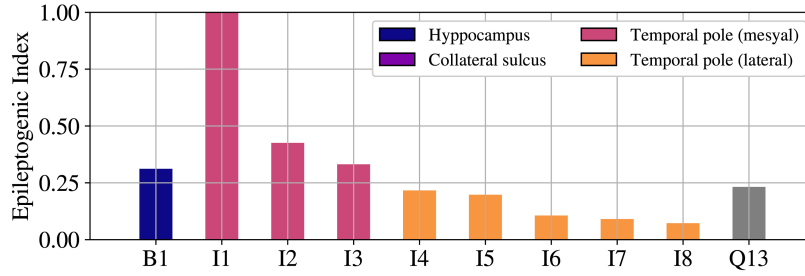


(b) Desynchronization level.

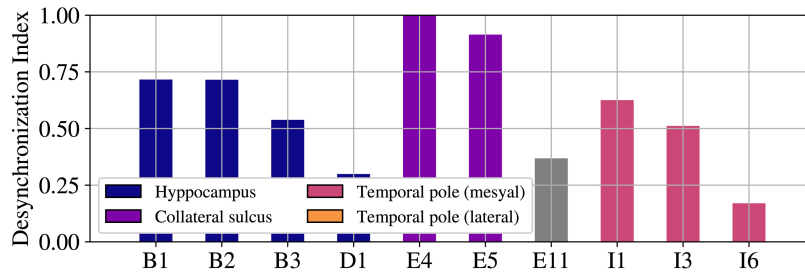
Fig. 8. DI operation in a discordant case (patient 8).

baseline and then increases abruptly during the ictal phase. In particular, the channels associated with electrode I, which crosses the temporal pole, maximize the energy ratio a few seconds after  $t_{start}$ .

In Fig. 8, we show the results obtained using the desynchronization level as the epileptogenic marker. In this case, the network connectivity is slightly less noisy than the seizure analyzed in Fig. 5 since the channels do not show prominent variations during the baseline period. This difference may be due to the different network sizes: the SEEG implant of patient 8 includes 36 more recording sites than that of patient 7. In other words, the



(a) EI.



(b) DI.

Fig. 9. EI and DI outcomes in a discordant case (patient 8).

SEEG implant explores a much more focused epileptogenic network and, thus, leads to a more stable connectivity dynamics.

Focusing on the ictal phase ( $t_{\text{start}} > 0$ ), we can appreciate that DI identifies desynchronization phenomena in several structures that, instead, are not marked by epileptogenic in terms of energy ratio. As shown in Fig. 8, channels associated with electrodes B, D, and E (which explore the cortical area adjacent the hippocampus and collateral sulcus) are characterized by a significant decrease in connectivity a few seconds after the start of the ictal phase. None of these channels (but B1) was included in those marked by EI, which can lead to the definition of a more restricted resection area during epilepsy surgery, with a lower chance of totally suppressing the mechanisms underlying seizure activation.

Fig. 9 compares the epileptogenicity levels assigned to each channel by the algorithms, also reporting the cortical locations of the channels within the SEEG implant. In this case, the output of the algorithm is only partially concordant: EI marked the channels associated with the temporal pole as the most epileptogenic, while DI seems to identify the origin of epileptic discharges in the limbic system. Using EI, the most epileptogenic channel is I1, while the algorithm DI places more emphasis on channel B1, B2, E4 and E5. These heterogeneous results denote the importance of integrating multiple techniques, considering both energy-based and connectivity-based metrics, to improve accuracy in the EZ localization.

#### 5.4 Clinical Discussion

Our results show that the DI algorithm can recognize the desynchronization phenomena that precede the propagation of epileptic discharge in electrodes that intersect or surround the EZ. This leads DI to have a

partially concordant output with EI, which, notably, aims to quantify the magnitude of the high-frequency energy associated with ictal activities. Contrary to EI and most state-of-the-art solutions, DI does not compute the signal energy over specific frequency bands, but evaluates the desynchronization level of each SEEG channel considering all its oscillatory components. This makes it possible to implement the algorithm in a patient-agnostic fashion, without the need for assumptions about the frequency ranges characterizing ictal phenomena. Tuning DI over a specific frequency range is also possible and may further improve the accuracy of our methodology. At the same time, adopting a frequency-specific solution may constitute a bias and reduce the generalizability of the framework.

When combined with EI, the DI algorithm allows us to greatly improve the accuracy in EZ localization. From a practical perspective, DI marks as epileptogenic the cortical sites that assume a static phase distribution over time and, thus, are not influenced by any other sites explored through the SEEG implant. The key idea behind our methodology is that epileptogenic signals present an independent behavior that cannot be inhibited by the other cortical structures. This is in line with the most recent findings in the field of EZ detection and confirms that the generation of epileptic seizures is allowed by a sudden reduction in network connectivity [13, 28, 29]. In this vision, the regions surrounding the EZ assume an inhibitory function that prevent epileptic discharges during the interictal phase.

In a clinical context, DI is not intended to directly plan the resection area for epilepsy surgery, but to help neurophysiologists identify the cortical sites that contribute to the propagation of epileptic discharges. In particular, DI emphasizes phenomena that are not marked by other computational techniques, such as EI, and are not easy to identify by a pure visual analysis. The combined use of DI and EI can strongly increase sensitivity in the detection of epileptogenic sites and can be used to reduce the number of SEEG channels that must be reviewed in practical scenarios. At the same time, the clinical judgment of neurophysiologists remains an essential element to discern false and true positive, counterbalancing the lower precision of our framework. In this regard, we remark that discerning ictal and non-ictal channels in a limited set, as the one given by our framework is a rather low-cost task, while reviewing all the SEEG channels is highly expensive and may lead to fatal human errors.

Finally, we observe that the DI algorithm may also reflect the presence of ictal activities in cortical areas not directly explored by the SEEG implant. This may be useful in scenarios where the SEEG signal does not provide a clear visualization of the ictal transition and the propagation of the seizures. Therefore, our framework can help neurophysiologists discern whether the epileptogenic network is totally or partially explored by the SEEG implant and, thus, the information obtained from the data is sufficient to ensure, with high probability, the success of epilepsy surgery.

## 6 Conclusion

In this work, we developed a new computational framework for analyzing SEEG signals, with the final goal of identifying EZ in patients with drug-resistant epilepsy. Our method, named DI, uses PTE to estimate the effective connectivity between the SEEG cortical sites and considers as epileptogenic the SEEG channels that present an abrupt desynchronization in the period immediately preceding the propagation of seizures. To evaluate its clinical utility, we implemented DI on a dataset of 11 patients and compared its performance in identifying epileptogenic sites against the EI algorithm. The results showed that DI leads to a higher AUC than EI in the EZ identification ( $AUC = 0.81$  vs  $AUC = 0.74$ ), and the best performance ( $AUC = 0.87$ ) is obtained when combining the two algorithms as a unique detection tool.

Our approach, integrated with other quantitative biomarkers, may constitute a key support for SEEG interpretation. The DI algorithm underscores signal modifications that are not visually evident, helping to identify those sites that contribute to the propagation of seizures or inhibit the epileptic discharge during the inter-ictal period. In future work, we intend to clinically validate the DI algorithm on a wider dataset, possibly including data from

different clinical research centers, and evaluate the potential of our computational framework for analyzing SEEG signals during the inter-ictal period.

## References

- [1] Nan An, Xiaolai Ye, Qiangqiang Liu, Jiwen Xu, and Puming Zhang. 2020. Localization of the epileptogenic zone based on ictal stereo-electroencephalogram: Brain network and single-channel signal feature analysis. *Epilepsy Research* 167 (Nov. 2020), 1–10.
- [2] Luiz A Baccalá and Koichi Sameshima. 2001. Partial directed coherence: a new concept in neural structure determination. *Biological Cybernetics* 84, 6 (Jun. 2001), 463–474.
- [3] Alexandra Balatskaya et al. 2020. The “Connectivity Epileptogenicity Index”(cEI), a method for mapping the different seizure onset patterns in StereoElectroEncephalography recorded seizures. *Clinical Neurophysiology* 131, 8 (Aug. 2020), 1947–1955.
- [4] Fabrice Bartolomei et al. 2017. Defining epileptogenic networks: contribution of SEEG and signal analysis. *Epilepsia* 58, 7 (Jul. 2017), 1131–1147.
- [5] Fabrice Bartolomei, Patrick Chauvel, and Fabrice Wendling. 2008. Epileptogenicity of brain structures in human temporal lobe epilepsy: a quantified study from intracerebral EEG. *Brain* 131, 7 (Jul. 2008), 1818–1830.
- [6] Fabrice Bartolomei, Anca Nica, Maria Paola Valenti-Hirsch, Claude Adam, and Marie Denuelle. 2017. Interpretation of SEEG recordings. *Neurophysiologie Clinique* 48, 1 (Dec. 2017), 53–57.
- [7] Fabrice Bartolomei, Fabrice Wendling, Jean-Jacques Bellanger, Jean Régis, and Patrick Chauvel. 2001. Neural networks involving the medial temporal structures in temporal lobe epilepsy. *Clinical Neurophysiology* 112, 9 (Sep. 2001), 1746–1760.
- [8] André M Bastos and Jan-Mathijs Schoffelen. 2016. A tutorial review of functional connectivity analysis methods and their interpretational pitfalls. *Frontiers in Systems Neuroscience* 9, 175 (Jan. 2016), 1–23.
- [9] John M. Bernabei et al. 2021. Electroocorticography and stereo EEG provide distinct measures of brain connectivity: implications for network models. *Brain Communications* 3, 3 (Jul. 2021), 1–11.
- [10] Abhijit Bhattacharyya, Radu Ranta, Steven Le Cam, Valerie Louis-Dorr, Louise Tyvaert, Sophie Colnat-Coulbois, Louis Maillard, and Ram Bilas Pachori. 2019. A Multi-Channel Approach for Cortical Stimulation Artefact Suppression in Depth EEG Signals Using Time-Frequency and Spatial Filtering. *IEEE Transactions on Biomedical Engineering* 66, 7 (Jul. 2019), 1915–1926.
- [11] Francesco Cardinale et al. 2015. Cerebral angiography for multimodal surgical planning in epilepsy surgery: description of a new three-dimensional technique and literature review. *World Neurosurgery* 84, 2 (Aug. 2015), 358–367.
- [12] Francesco Cardinale, Massimo Cossu, Laura Castana, Giuseppe Casaceli, Marco Paolo Schiariti, Anna Misericocchi, Dalila Fuschillo, Alessio Moscato, Chiara Caborni, Gabriele Arnulfo, et al. 2013. Stereoelectroencephalography: surgical methodology, safety, and stereotactic application accuracy in 500 procedures. *Neurosurgery* 72, 3 (Mar. 2013), 353–366.
- [13] Stefania Coelli, Eleonora Maggioni, Annalisa Rubino, Chiara Campana, Lino Nobili, and Anna M. Bianchi. 2019. Multiscale Functional Clustering Reveals Frequency Dependent Brain Organization in Type II Focal Cortical Dysplasia With Sleep Hypermotor Epilepsy. *IEEE Transactions on Biomedical Engineering* 66, 10 (2019), 2831–2839. <https://doi.org/10.1109/TBME.2019.2896893>
- [14] Massimo Cossu, Francesco Cardinale, Laura Castana, Alberto Citterio, Stefano Francione, Laura Tassi, Alim L Benabid, and Giorgio Lo Russo. 2005. Stereoelectroencephalography in the presurgical evaluation of focal epilepsy: a retrospective analysis of 215 procedures. *Neurosurgery* 57, 4 (Oct. 2005), 706–718.
- [15] Maëva Daoud et al. 2022. Stereo-EEG based personalized multichannel transcranial direct current stimulation in drug-resistant epilepsy. *Clinical Neurophysiology* 137 (May 2022), 142–151.
- [16] Olivier David et al. 2011. Imaging the seizure onset zone with stereo-electroencephalography. *Brain* 134, 10 (Oct. 2011), 2898–2911.
- [17] David Freedman and Persi Diaconis. 1981. On the histogram as a density estimator: L 2 theory. *Zeitschrift für Wahrscheinlichkeitstheorie und verwandte Gebiete* 57, 4 (Dec. 1981), 453–476.
- [18] Vadym Gnatkovsky et al. 2014. Biomarkers of epileptogenic zone defined by quantified stereo-EEG analysis. *Epilepsia* 55, 2 (Feb. 2014), 296–305.
- [19] Olesya Grinenko, Jian Li, John C Mosher, Irene Z Wang, Juan C Bulacio, Jorge Gonzalez-Martinez, Dileep Nair, Imad Najm, Richard M Leahy, and Patrick Chauvel. 2017. A fingerprint of the epileptogenic zone in human epilepsies. *Brain* 141, 1 (12 2017), 117–131.
- [20] Kristin M. Gunnarsdottir et al. 2022. Source-sink connectivity: A novel interictal EEG marker for seizure localization. *Brain* 145, 11 (Nov. 2022), 3901–3915.
- [21] Jiayang Guo et al. 2021. Detecting High Frequency Oscillations for Stereoelectroencephalography in Epilepsy via Hypergraph Learning. *IEEE Transactions on Neural Systems and Rehabilitation Engineering* 29 (2021), 587–596. <https://doi.org/10.1109/TNSRE.2021.3056685>
- [22] Kanupriya Gupta, Pulkit Grover, and Taylor J Abel. 2020. Current conceptual understanding of the epileptogenic network from stereoelectroencephalography-based connectivity inferences. *Frontiers in Neurology* 11, 569699 (Nov. 2020), 1–7.
- [23] David W Hosmer Jr, Stanley Lemeshow, and Rodney X Sturdivant. 2013. *Applied logistic regression*. John Wiley & Sons.
- [24] Shuaicong Hu et al. 2023. Exploring the Applicability of Transfer Learning and Feature Engineering in Epilepsy Prediction Using Hybrid Transformer Model. *IEEE Transactions on Neural Systems and Rehabilitation Engineering* 31 (2023), 1321–1332. <https://doi.org/10.1109/>

- TNSRE.2023.3244045
- [25] Yali Huang et al. 2023. Intracranial electrophysiological and structural basis of BOLD functional connectivity in human brain white matter. *Nature Communications* 14, 3414 (Jun. 2023), 1–9.
- [26] Amir Hussein, Marc Djandji, Reem A. Mahmoud, Mohamad Dhaybi, and Hazem Hajj. 2020. Augmenting DL with Adversarial Training for Robust Prediction of Epilepsy Seizures. *ACM Trans. Comput. Healthcare* 1, 3 (Jun. 2020), 1–18.
- [27] Jean Isnard et al. 2018. French guidelines on stereoelectroencephalography (SEEG). *Neurophysiologie Clinique* 48, 1 (Feb. 2018), 5–13.
- [28] Haiteng Jiang et al. 2022. Interictal SEEG resting-state connectivity localizes the seizure onset zone and predicts seizure outcome. *Advanced Science* 9, 2200887 (Jun. 2022), 1–11.
- [29] Graham W Johnson et al. 2023. The Interictal Suppression Hypothesis in focal epilepsy: network-level supporting evidence. *Brain* 146, 7 (Feb. 2023), 2828–2845.
- [30] Jean-Philippe Lachaux, Eugenio Rodriguez, Jacques Martinerie, and Francisco J Varela. 1999. Measuring phase synchrony in brain signals. *Human Brain Mapping* 8, 4 (Nov. 1999), 194–208.
- [31] Chunsheng Li, Abbas Sohrabpour, Haiteng Jiang, and Bin He. 2021. High-Frequency Hubs of the Ictal Cross-Frequency Coupling Network Predict Surgical Outcome in Epilepsy Patients. *IEEE Transactions on Neural Systems and Rehabilitation Engineering* 29 (2021), 1290–1299. <https://doi.org/10.1109/TNSRE.2021.3093703>
- [32] Xiaotong Liu, Fang Han, Rui Fu, Qingyun Wang, and Guoming Luan. 2021. Epileptogenic zone location of temporal lobe epilepsy by cross-frequency coupling analysis. *Frontiers in Neurology* 12, 764821 (Nov. 2021), 1–14.
- [33] Muriel Lobier, Felix Siebenhühner, Satu Palva, and J Matias Palva. 2014. Phase transfer entropy: a novel phase-based measure for directed connectivity in networks coupled by oscillatory interactions. *Neuroimage* 85, 2 (Jan. 2014), 853–872.
- [34] Hans O Lüders, Imad Najm, Dileep Nair, Peter Widdess-Walsh, and William Bingman. 2006. The epileptogenic zone: general principles. *Epileptic Disorders* 8, 2 (Aug. 2006), 1–9.
- [35] Julia Makhalova et al. 2023. The role of quantitative markers in surgical prognostication after stereoelectroencephalography. *Annals of Clinical and Translational Neurology* 10, 11 (Nov. 2023), 2114–2126.
- [36] Douglas C Montgomery. 2019. *Introduction to statistical quality control*. John Wiley & Sons.
- [37] G Nithin, PS Sathidevi, and PM Ameer. 2021. Graph energy based centrality measures to detect epileptogenic focal invasive EEG electrodes. *Seizure* 85 (Feb. 2021), 127–137.
- [38] Harilal Parasuram, Siby Gopinath, Ashok Pillai, Shyam Diwakar, and Anand Kumar. 2021. Quantification of epileptogenic network from stereo EEG recordings using epileptogenicity ranking method. *Frontiers in Neurology* 12 (2021), 738111.
- [39] Luis R Peraza, Aziz UR Asghar, Gary Green, and David M Halliday. 2012. Volume conduction effects in brain network inference from electroencephalographic recordings using phase lag index. *Journal of Neuroscience Methods* 207, 2 (Jun. 2012), 189–199.
- [40] Timothée Proix, Fabrice Bartolomei, Maxime Guye, and Viktor K Jirsa. 2017. Individual brain structure and modeling predict seizure propagation. *Brain* 140, 3 (Mar. 2017), 641–654.
- [41] Nicolas Roehri, Jean-Marc Lina, John C. Mosher, Fabrice Bartolomei, and Christian-George Bénar. 2016. Time-Frequency Strategies for Increasing High-Frequency Oscillation Detectability in Intracerebral EEG. *IEEE Transactions on Biomedical Engineering* 63, 12 (2016), 2595–2606. <https://doi.org/10.1109/TBME.2016.2556425>
- [42] Ali Shojaie and Emily B Fox. 2022. Granger causality: A review and recent advances. *Annual Review of Statistics and Its Application* 9, 1 (Mar. 2022), 289–319.
- [43] Ross Sparks and James D Wilson. 2019. Monitoring communication outbreaks among an unknown team of actors in dynamic networks. *Journal of Quality Technology* 51, 4 (Oct. 2019), 353–374.
- [44] Cornelis J Stam, Guido Nolte, and Andreas Daffertshofer. 2007. Phase lag index: assessment of functional connectivity from multi channel EEG and MEG with diminished bias from common sources. *Human Brain Mapping* 28, 11 (Nov. 2007), 1178–1193.
- [45] Elena Urrestarazu, Rahul Chander, François Dubeau, and Jean Gotman. 2007. Interictal high-frequency oscillations (100–500 Hz) in the intracerebral EEG of epileptic patients. *Brain* 130, 9 (Jul. 2007), 2354–2366.
- [46] Meng-yang Wang et al. 2017. Identification of the epileptogenic zone of temporal lobe epilepsy from stereo-electroencephalography signals: A phase transfer entropy and graph theory approach. *NeuroImage: Clinical* 16 (Jul. 2017), 184–195.
- [47] Fabrice Wendling, Jean-Jacques Bellanger, Fabrice Bartolomei, and Patrick Chauvel. 2000. Relevance of nonlinear lumped-parameter models in the analysis of depth-EEG epileptic signals. *Biological cybernetics* 83, 4 (Oct. 2000), 367–378.
- [48] Xiaolong Wu, Guangye Li, Xin Gao, Benjamin Metcalfe, and Dingguo Zhang. 2024. Channel Selection for Stereo- Electroencephalography (SEEG)-Based Invasive Brain-Computer Interfaces Using Deep Learning Methods. *IEEE Transactions on Neural Systems and Rehabilitation Engineering* 32 (2024), 800–811. <https://doi.org/10.1109/TNSRE.2024.3364752>
- [49] Jerrold H Zar. 2005. Spearman rank correlation. *Encyclopedia of Biostatistics* 7 (Jul. 2005), 1–6.